Aluminium oxide formation via atomic layer deposition using a polymer brush mediated selective infiltration approach

M. Snelgrove[1], C. McFeely[1], P.G. Mani-Gonzalez[2], K. Lahtonen[3], R. Lundy[4], G. Hughes[1,5], M. Valden[6], E. McGlynn[1,5], P. Yadav[4], J. Saari[6], M. A. Morris[4] and R. O´Connor[1]

[1]*School of Physical Sciences, Dublin City University, Dublin 9, Ireland*

[2]*Instituto de Ingeniería y Tecnología, Departamento de Física y Matemáticas, Universidad Autónoma de Ciudad Juárez, Ave. Del Charro 450, Cd. Juárez C.P. 32310, Chihuahua. México.*

[3]*Faculty of Engineering and Natural Sciences, Tampere University, P.O. Box 692, FI-33014 Tampere, Finland*

[4] *AMBER Research Centre and School of Chemistry, Trinity College Dublin, Dublin 2, Ireland*

[5]*National Centre for Plasma Science and Technology, Dublin City University, Glasnevin, Dublin 9, Ireland*

[6]*Surface Science Group, Photonics Laboratory, Tampere University, P.O. Box 692, FI-33014 Tampere, Finland*

Abstract

Area selective deposition (ASD) is an emerging method for the patterning of electronic devices as it can significantly reduce processing steps in the industry. A potential ASD methodology uses infiltration of metal precursors into patterned polymer materials. The work presented within demonstrates this potential by examining hydroxy terminated poly(2-vinylpyridine) (P2VP-OH) as the 'receiving' polymer and trimethylaluminium (TMA) and H_2O as the material precursors in a conventional atomic layer deposition (ALD) process. Fundamental understanding of the surface process was achieved using X-ray photoelectron spectroscopy (XPS) and energy dispersive X-ray spectroscopy (EDX) mapping via transmission electron microscopy (TEM). The resulting analysis confirms aluminium inclusion within the polymer film. Spectroscopic and microscopic characterisation show metal infiltration throughout the polymer to the underlying silicon dioxide interface. Exposing the infiltrated film to an oxygen plasma results in the removal of the organic component and resultant fabrication of a sub 5 nm aluminium oxide layer.

Introduction

Research into 'bottom up' lithography methods as an alternative to conventional 'top down' patterning techniques for next-generation electronic devices has led to major efforts in identifying suitable polymers for block copolymer (BCP) lithography [1–3], and, more recently, area selective deposition [4,5]. The study of polymers that are receptive to infiltration of subsequently deposited materials, and that demonstrate the capacity for use in BCP or selective area type patterns, is a growing area of research [6,7]. Poly(2-vinylpyridine) (P2VP) is an attractive polymer having properties that make it prototypical for patterning and infiltration processes [7–9]. These advantages are apparent as pyridine-based polymers are ideal for infiltration because of the nitrogen lone pair and it should be noted that systems such as polystyrene-poly(vinylpyridine) are capable of patterning at extreme dimensions (<

10 nm) [10]. However, the potential of PVP systems as an infiltration media is much less studied than the intensively studied PMMA (Poly(methyl methacrylate)) [10]. Because of the interest in PVP as a potential acceptor, recent work has shown progress in its use via rapid, high-quality grafting of the polymer as a brush layer, and its infiltration with Al through a liquid phase approach [11]. Our previous studies have concentrated on the surface characterisation of these P2VP-OH brushes [12], and the capacity that these films have in facilitating infiltration via a Cu salt (liquid phase) inclusion process [13].

While a liquid phase infiltration approach into brush films has many benefits, vapor phase area selective infiltration techniques such as ALD have not yet been demonstrated using these brush type films. The focus of this work is on developing an area selective, ALD compatible deposition process using a covalently grafted P2VP-OH brush which could be patterned via conventional lithographic masking or by tailoring selective polymer brush end groups to bind to site specific wafer regions. This approach may have significant relevance for silicon device technologies, particularly in monolithic integration due to the low temperature ceiling (<500 °C) required for complementary metal–oxide–semiconductor (CMOS) compatibility [14].

The vapor phase ALD technique, in which chemical precursors and reactant gases are sequentially admitted to a deposition chamber under vacuum, is a film growth method that is regarded as highly conformal and controllable [15], with applications in a wide range of nanopatterning fields including ASD and BCPs [16]. Traditional ALD methods were based on depositing a material on top of a substrate, however it is important to note - that for ASD and BCP ALD approaches - infiltration into the polymer film is often desired. Numerous studies have been performed on blanket polymer films and BCPs in order to produce metal oxide films and nanopatterns respectively, with several alterations from the standard ALD cycle growth used in achieving infiltration. A review by C. Leng and M. Losego [17] outlined three of these alternative techniques for polymer infiltration – semi-static sequential infiltration synthesis (SIS)[18–20], flow mode SIS [21] and sequential vapor infiltration (SVI) [22]. Despite operational differences, all three operate by means of holding precursors and/or co-reactants in the chamber for a designated amount of time – unlike in the non-stagnated approach in conventional ALD.

While these methods have achieved positive results, conventional ALD cycle growth has also been extensively reported to achieve infiltration into polymer films [23–25]. The work presented here demonstrates complete Al infiltration into a P2VP-OH film, with the avoidance of the longer cycle time experienced in a SIS approach. Aluminium was chosen as the material for infiltration, as there is extensive knowledge in the fabrication of Al_2O_3 thin films via ALD, both through deposition on surfaces and through infiltration into various polymers [26,27]. Precursor infiltration and metal coordination to the polymer is expected due to the strong chemical interaction between Al and pyridine [28,29]. Alumina is a high-dielectric constant (high-k) material that excels as a diffusion barrier with good thermal stability, resulting in it having a wide-range of uses in the semiconductor industry [30,31]. EDX mapping confirms the ability of P2VP to facilitate metal incorporation with this technique, and the XPS analysis allows for a detailed study of the environment of the surface after infiltration. An *in-situ*

oxygen plasma step was performed post ALD infiltration, to produce and study the resultant Al-oxide layer on the Si oxide surface after polymer removal.

Experimental

P2VP-OH (P7544-2VPOH) (PDI: 1.05) with a molecular weight of 6 kg mol^{-1} was purchased from Polymer Source. The P2VP-OH was dissolved in tetrahydrofuran (THF) and subsequently spin-coated onto Si substrates in accordance with reference [11] to yield approximately 4 nm thick polymer films. Aluminium infiltration into the P2VP-OH film via ALD was performed in a commercial reactor (Picosun Sunale ALD R200 Advanced reactor), using TMA and H_2O as precursors and N_2 as the carrier gas. The substrate was heated to a temperature of 200°C (well within polymer thermal stability) and a recipe was implemented that would normally be expected to yield a 2 nm thick film of Al_2O_3 on a blanket, OH terminated Si surface. One cycle consisted of a 0.1 s TMA pulse followed by a 3 s N_2 purge. This was then followed by a 0.1 s H_2O pulse followed by a 4 s N_2 purge. N_2 was continuously flowed through the TMA and H_2O lines at 150 sccm and 200 sccm respectively. A total of 20 cycles were performed.

XPS data was obtained using a ThermoFisher-VG instrument equipped with an Al Kα (*hv* = 1486.7 eV) X-ray source and a 3-channeltron hemispherical electron analyser (base pressure; 1×10^{-9} mbar). XPS data analysis was performed using AAnalyzer [32], with spectra fitted using the simultaneous fit method and by using Voigt functions. All XPS spectra were shifted so that the Si $2p_{3/2}$ component was located at 99.4 eV [33,34]. The oxygen plasma process was performed in a purpose built chamber with a custom made plasma source coupled with the XPS analysis chamber, to ensure the sample did not have to break vacuum after the polymer removal / metal oxidation step. The plasma process took place in a pressure of 1×10^{-2} - 2×10^{-2} mbar of oxygen at 30 W for 600 s.

Sample preparation for TEM (FEI OSIRIS TEM) and subsequent EDX cross section imaging was undertaken in a FEI Helios Nanolab 450 S. Samples were capped with Pt via a gas injection system.

Results

XPS

Photoemission analysis was performed on the P2VP-OH films pre- and post-ALD deposition, as well as after oxygen plasma processing to examine the effects of polymer removal and metal oxidation. The XPS intensity of the relevant core levels at each stage of the fabrication process (sample of P2VP as received, sample of P2VP after ALD, sample after oxygen plasma) are shown in Figure 1. XPS spectra of the N 1*s* and C 1*s* (Figure S1 and S2 respectively, supporting information) reveal the presence of the P2VP film before and after the ALD step, with the significant loss in intensity (Figure 1 (a)) after the oxygen plasma step attributed to the polymer being removed.

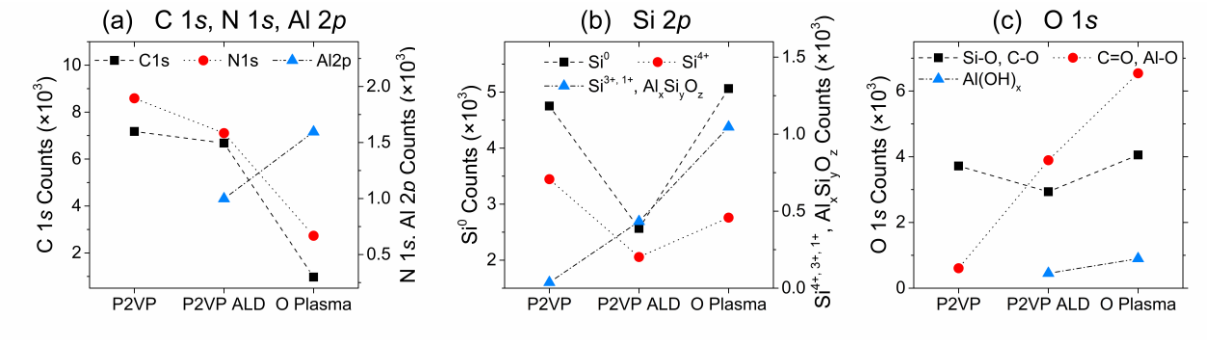

Figure 1: XPS counts of the (a) C 1s, N 1s & Al 2p, (b) Si 2p and (c) O 1s core levels for the polymer pre and post ALD, and post O plasma processing. The counts presented are non-normalized and obtained from area under the curve calculations.

The spectra of the Si 2*p* and Al 2*p* results are shown in Figure 2 (a). For the P2VP film prior to ALD deposition, no Al is present, and the Si 2*p* spectra is dominated by the Si bulk and Si^{4+} signal, with the $2p_{3/2}$ elements located at 99.4 and 103.4 eV binding energy, respectively. Post ALD processing, the TMA appears to have reacted with the P2VP film, with the Al 2*p* maxima occurring at 75.1 eV binding energy. The Al 2*p* peak was not fitted due to the unresolvable splitting distance of 0.4 eV between the $2p_{1/2}$ and $2p_{3/2}$ components. P2VP can undergo chemical coordination with metal species, facilitated by the electron lone pair in the polymer's pyridinic N [35–37]. It is believed that the Al exists in a complex multi – oxidised state at this stage which includes Al - pyridinyl nitrogen bonding [38]. This type of metal – pyridine bonding has been observed for the P2VP-OH brush films that have been infiltrated with Cu through a liquid phase infiltration process [13].

Following the ALD process, Si^{1+} and Si^{3+} components become apparent in the Si 2*p* fit, with the $2p_{3/2}$ elements located at 100.4 and 101.9 eV binding energy, respectively (inset Figure 2a). These peak positions are consistent with the binding energies of Si suboxide states as reported by Himpsel et al [39]. Another peak, it's $2p_{3/2}$ component located at 103.0 eV binding energy, was required to obtain an accurate curve fit to the raw data, and, combined with the presence of Si^{1+} and Si^{3+} oxides, represents evidence of the interaction of the Al precursor with the SiO_2 layer, resulting in the formation of Al-silicates ($Al_xSi_yO_z$) at the polymer-SiO_2 interface. This confirms that the Al has fully penetrated the polymer film and chemically interacted with the SiO_2 layer.

The O 1*s* spectra in Figure 2 (b) for the P2VP film is made up of two components – the predominant signal at 532.6 eV binding energy represents a combination of C-O bonds in the polymer chain and Si-O bonds (SiO_2 and Si sub oxides) in the layer below. The signal at 531.6 eV binding energy is associated with carbon oxygen bonds that have arisen due to atmospheric exposure [13,40,41]. After ALD deposition, the peak profile of the O 1*s* significantly broadens. The Si-O (now also representing $Al_xSi_yO_z$ bonds), C-O signal coexists with two other components located at 531.7 and 533.7 eV binding energy. The former, fitted with a larger Gaussian component, represents a combination of C=O and oxidised Al bonds, while the latter represents hydroxyl Al groups [42,43].

The oxygen plasma treatment results in a rise in counts for both the Si 2*p* and Al 2*p* signals (Figure 1 (a) & (b)), linked to the removal of the polymer film as evident by the significant reduction in the C 1*s* and N 1*s* signals after in situ processing. The Si^{1+} and Si^{3+} sub oxides

remain, along with the $Al_xSi_yO_z$ component at 103.0 eV binding energy. The maximum of the Al 2*p* shifts 0.4 eV to 75.5 eV binding energy, which is consistent with the position of Al_2O_3 reported in other studies [43,44]. However, the reported Al 2*p* binding energy of Al_2O_3 varies considerably in the literature [42,45–47] and as such the exact stoichiometry of the film is uncertain. While the binding energy and stoichiometry is debated, it is apparent that the observed shift to higher binding energy suggests a transition from a lower to higher oxidation state [48], and the substantial reduction in C and N signals confirms that a pure Al-oxide layer (Al_xO_y) remains above the SiO_2 layer. For the O 1*s*, Al-O bonds now dominate the spectra, at the expense of the Si-O, C-O component due to polymer removal (Figure 1 (c)). A rise in hydroxyl Al groups is also observed. We note that the area of the Si-O/C-O component increases, consistent with the presence of a thin layer of Al oxide on the Si substrate, and this increase in intensity (from the SiO_2 and Si sub-oxides signals) is greater than the intensity loss that the component experiences due to the removal of C-O bonds.

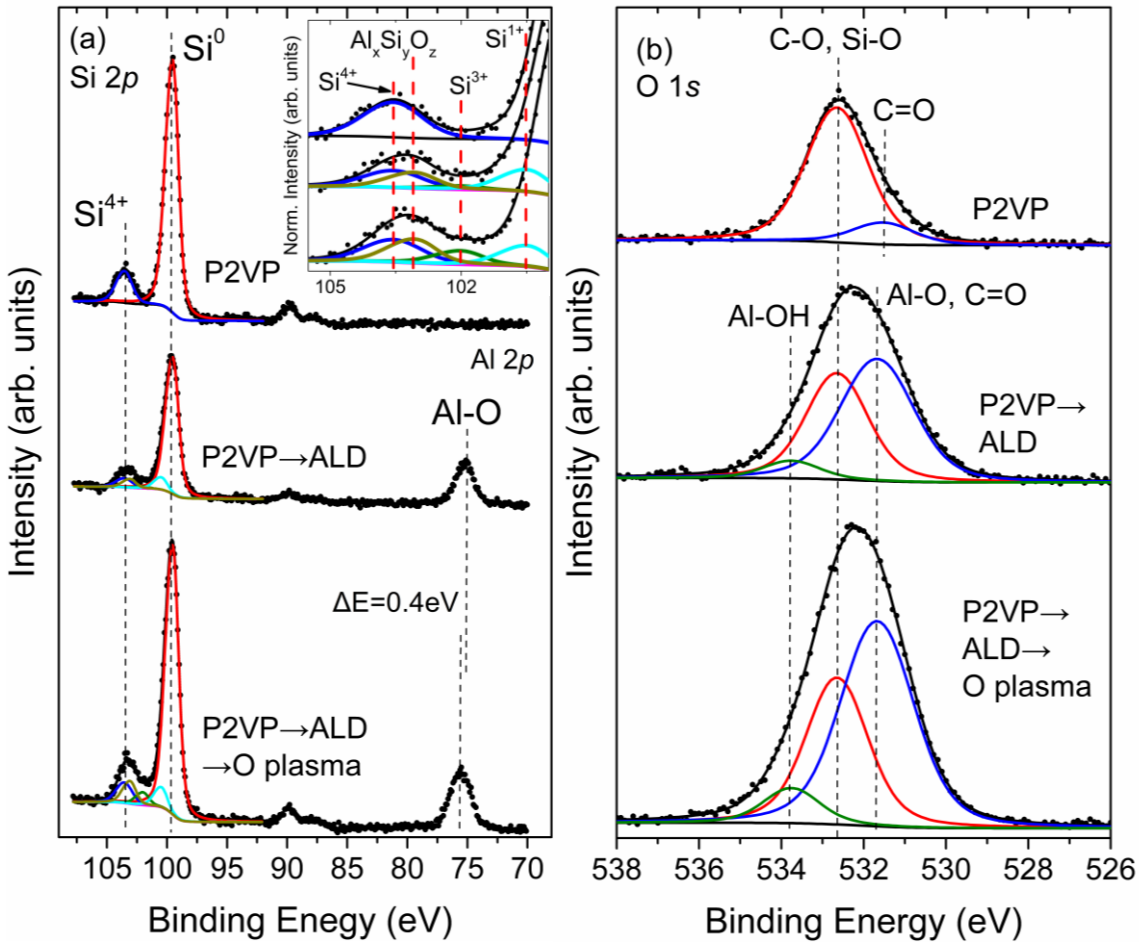

Figure 2 (a): XPS spectra of the Si 2p and Al 2p. Al is observed after ALD processing, and shifts to a higher binding energy after the O plasma treatment. The Si 2p spectra shows evidence of sub oxide formation after the ALD step, suggesting Al interaction with the SiO_2 layer. (b): O 1s XPS spectra. The peak sees significant broadening post ALD with the addition of Al-O bonds, with this signal dominating after the O plasma step.

TEM & EDX

TEM and EDX cross sections of the fabricated P2VP-OH films in the outlined process has previously revealed that the resultant polymer films are ~4 nm in thickness [12]. The images

in Figure 3 show the resultant cross sections arising from the ALD and oxygen plasma process. The EDX mapping/TEM imaging of P2VP after the ALD process in Figure 3 (a-c) reveals that the Al exists in the polymer layer showing that the metal has infiltrated into the P2VP and has not been limited to growth on top of the film. The mapping images also show that the Al signal has reached the SiO_2/P2VP interface. This correlates with the appearance of sub oxides and Al silicates in the insert of Figure 2 (a) for the Si 2*p* fit consistent with Al interacting with the SiO_2 layer at the P2VP/SiO_2 interface.

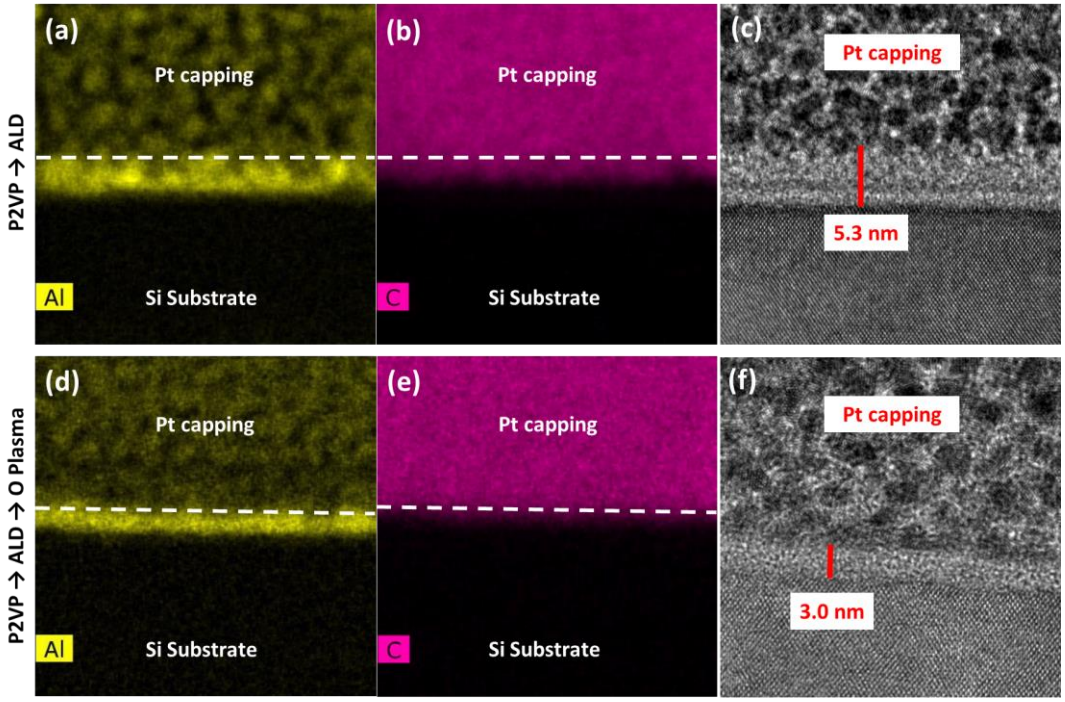

Figure 3: EDX Al and C mapping images ((a), (b) respectively) and TEM (c) of the P2VP-OH film after ALD deposition. Both Al and C signals are detected in the film above the Si. EDX mapping of Al (d) and C (e) and TEM after O plasma processing (f)). A uniform Al film of 3nm is observed with no C signal detected. The white dashed line in the EDX images shows where the Pt cap ends, and the film begins.

The EDX and TEM images of the film following oxygen plasma processing in Figure 3 (d-f) reveal that a thin, uniform film of Al oxide now resides on the Si substrate, with no carbon remaining in the film, correlating with the XPS results. Furthermore, the decrease in film thickness is consistent with the subsequent increase in intensity for the Si^0 and Si sub-oxide components as seen in the photoemission spectra.

Conclusion

By optimizing a conventional, relatively quick ALD process, thin layers of Al oxide have been successfully grown through the infiltration of a P2VP film, without the need for precursor hold times found in SIS-like approaches. Clear evidence of the brush layer being receptive to aluminium via a TMA and H_2O recipe has been reported for the first time. Further work is now required to optimize the reported process for maximum precursor infiltration into the polymer. XPS and EDX-TEM cross-sectioning reveals that Al resides within the polymer film all the way through to the SiO_2 interface, confirming that the brush layer is highly receptive to TMA infiltration. The reported results show a unique way of confirming whether a potential acceptor material can be entirely infused with a metal, through the detection of precursor

interaction with the underlying substrate. A fast, simple oxygen plasma ashes the polymer and oxidises the Al, creating a uniform metal oxide layer. This concludes that thin brush layers can be quickly removed, without the loss of the ALD-infiltrated metal. The in-situ aspect of this process allows for the confirmation that polymer removal is complete. These results highlight the promising potential that P2VP and other brush films have in future ASD processes that seek to implement rapid ALD methods for device fabrication.

Acknowledgements

This work has been facilitated with the financial support of Science Foundation Ireland (SFI) under Grant No. 12/RC/2278 and 16/SP/3809, and from the World Technology Universities Network (WTUN, under the WTUN Exchanges Programme). J.S. was supported by the Vilho, Yrjö and Kalle Väisälä Foundation of the Finnish Academy of Science and Letters. The research done in the Surface Science Group was supported by the Academy of Finland Flagship Programme, Photonics Research and Innovation (PREIN) (Decision No 320165), by Jane & Aatos Erkko Foundation (project 'SOFUS') and by Business Finland (decision No 1464/31/2019). The authors would like to thank Alan Bell, David Bird, Chris O'Neill and Jennifer Mckenna, at Intel Ireland, Leixlip. Technical support from Mr. Patrick Wogan and Mr. Des Lavelle is greatly appreciated.

[1] C.J. Hawker, T.P. Russell, Block copolymer lithography: Merging "bottom-up" with "top-down" processes, MRS Bull. 30 (2005) 952–966. https://doi.org/10.1557/mrs2005.249.

[2] M.A. Morris, Directed self-assembly of block copolymers for nanocircuitry fabrication, Microelectron. Eng. 132 (2015) 207–217. https://doi.org/10.1016/j.mee.2014.08.009.

[3] C. Cummins, A. Bell, M. Morris, Creating Active Device Materials for Nanoelectronics Using Block Copolymer Lithography, Nanomaterials. 7 (2017) 304. https://doi.org/10.3390/nano7100304.

[4] C. Cummins, M.T. Shaw, M.A. Morris, Area Selective Polymer Brush Deposition, Macromol. Rapid Commun. 38 (2017) 1–6. https://doi.org/10.1002/marc.201700252.

[5] C. Cummins, T. Weingä, M.A. Morris, Enabling Large-Area Selective Deposition on Metal-Dielectric Patterns using Polymer Brush Deactivation, (2018). https://doi.org/10.1021/acs.jpcc.8b04092.

[6] C. Cummins, M.A. Morris, Using block copolymers as infiltration sites for development of future nanoelectronic devices: Achievements, barriers, and opportunities, Microelectron. Eng. 195 (2018) 74–85. https://doi.org/10.1016/j.mee.2018.04.005.

[7] P. Mokarian-Tabari, R. Senthamaraikannan, C. Glynn, T.W. Collins, C. Cummins, D. Nugent, ‖ Colm O'dwyer, M.A. Morris, Large Block Copolymer Self-Assembly for Fabrication of Subwavelength Nanostructures for Applications in Optics, (2017). https://doi.org/10.1021/acs.nanolett.7b00226.

[8] J.G. Kennemur, Poly(vinylpyridine) Segments in Block Copolymers: Synthesis, Self-Assembly, and Versatility, Macromolecules. 52 (2019) 1354–1370. https://doi.org/10.1021/acs.macromol.8b01661.

[9] G. Jang, A. Khan, C.J. Hawker, E.J. Kramer, Morphology Evolution of PS-b-P2VP Diblock Copolymers via Supramolecular Assembly of Hydroxylated Gold Nanoparticles, (2012). https://doi.org/10.1021/ma202391k.

[10] C. Sinturel, F.S. Bates, M.A. Hillmyer, High χ−Low N Block Polymers: How Far Can We Go?, 11 (2019) 40. https://doi.org/10.1021/acsmacrolett.5b00472.

[11] R. Lundy, P. Yadav, A. Selkirk, E. Mullen, T. Ghoshal, C. Cummins, M.A. Morris, R. Lundy, P. Yadav, A. Selkirk, E. Mullen, T. Ghoshal, C. Cummins, Optimizing polymer brush coverage to develop highly coherent sub-5nm oxide films by ion inclusion Optimizing polymer brush coverage to develop highly coherent sub- 5nm oxide films by ion inclusion, (2019). https://doi.org/10.1021/acs.chemmater.9b02856.

[12] M. Snelgrove, C. Zehe, R. Lundy, P. Yadav, J.-P. Rueff, R. O'Connor, J. Bogan, G. Hughes, E. McGlynn, M. Morris, P.G. Mani-Gonzalez, Surface characterization of poly-2-vinylpyridine—A polymer for area selective deposition techniques, J. Vac. Sci. Technol. A. 37 (2019) 050601. https://doi.org/10.1116/1.5115769.

[13] M. Snelgrove, P.G. Mani-Gonzalez, J. Bogan, R. Lundy, J.-P. Rueff, G. Hughes, P. Yadav, E. McGlynn, M. Morris, R. O'Connor, Hard x-ray photoelectron spectroscopy study of copper formation by metal salt inclusion in a polymer film, J. Phys. D. Appl. Phys. 52 (2019) 435301. https://doi.org/10.1088/1361-6463/ab35b2.

[14] F. Deprat, F. Nemouchi, C. Fenouillet-Beranger, M. Casse, P. Rodriguez, B. Previtali, N. Rambal, V. Delaye, M. Haond, M. Mellier, M. Gregoire, M. Danielou, S. Favier, P. Batude, M. Vinet, First integration of Ni0.9Co0.1 on pMOS transistors, in: 2016 IEEE Int. Interconnect Technol. Conf. / Adv. Met. Conf. IITC/AMC 2016, Institute of Electrical and Electronics Engineers Inc., 2016: pp. 133–135. https://doi.org/10.1109/IITC-AMC.2016.7507708.

[15] R.W. Johnson, A. Hultqvist, S.F. Bent, A brief review of atomic layer deposition: From fundamentals to applications, Mater. Today. 17 (2014) 236–246. https://doi.org/10.1016/j.mattod.2014.04.026.

[16] A.J.M. Mackus, A.A. Bol, W.M.M. Kessels, The use of atomic layer deposition in advanced nanopatterning, (2014). https://doi.org/10.1039/c4nr01954g.

[17] C.Z. Leng, M.D. Losego, Vapor phase infiltration (VPI) for transforming polymers into organic-inorganic hybrid materials: A critical review of current progress and future challenges, Mater. Horizons. 4 (2017) 747–771. https://doi.org/10.1039/c7mh00196g.

[18] Q. Peng, Y.C. Tseng, S.B. Darling, J.W. Elam, Nanoscopic patterned materials with tunable dimensions via atomic layer deposition on block copolymers, Adv. Mater. 22 (2010) 5129–5133. https://doi.org/10.1002/adma.201002465.

[19] Q. Peng, Y.C. Tseng, S.B. Darling, J.W. Elam, A route to nanoscopic materials via sequential infiltration synthesis on block copolymer templates, ACS Nano. 5 (2011)

4600–4606. https://doi.org/10.1021/nn2003234.

[20] Y.C. Tseng, Q. Peng, L.E. Ocola, D.A. Czaplewski, J.W. Elam, S.B. Darling, Enhanced polymeric lithography resists via sequential infiltration synthesis, J. Mater. Chem. 21 (2011) 11722–11725. https://doi.org/10.1039/c1jm12461g.

[21] M. Biswas, J.A. Libera, S.B. Darling, J.W. Elam, New insight into the mechanism of sequential infiltration synthesis from infrared spectroscopy, Chem. Mater. 26 (2014) 6135–6141. https://doi.org/10.1021/cm502427q.

[22] E.C. Dandley, C.D. Needham, P.S. Williams, A.H. Brozena, C.J. Oldham, G.N. Parsons, Temperature-dependent reaction between trimethylaluminum and poly(methyl methacrylate) during sequential vapor infiltration: Experimental and ab initio analysis, J. Mater. Chem. C. 2 (2014) 9416–9424. https://doi.org/10.1039/c4tc01293c.

[23] J.D. Ferguson, A.W. Weimer, S.M. George, Atomic Layer Deposition of Al 2 O 3 Films on Polyethylene Particles, (2004). https://doi.org/10.1021/cm040008y.

[24] J.C. Spagnola, B. Gong, S.A. Arvidson, J.S. Jur, S.A. Khan, G.N. Parsons, Surface and sub-surface reactions during low temperature aluminium oxide atomic layer deposition on fiber-forming polymers, (n.d.). https://doi.org/10.1039/c0jm00355g.

[25] R.P. Padbury, J.S. Jur, Effect of Polymer Microstructure on the Nucleation Behavior of Alumina via Atomic Layer Deposition, (2014). https://doi.org/10.1021/jp506456y.

[26] J.L. Van Hemmen, S.B.S. Heil, J.H. Klootwijk, F. Roozeboom, C.J. Hodson, M.C.M. Van De Sanden, W.M.M. Kessels, Plasma and thermal ALD of Al2O3 in a commercial 200 mm ALD reactor, J. Electrochem. Soc. 154 (2007). https://doi.org/10.1149/1.2737629.

[27] B. Gong, G.N. Parsons, Quantitative in situ infrared analysis of reactions between trimethylaluminum and polymers during Al 2O 3 atomic layer deposition, J. Mater. Chem. 22 (2012) 15672–15682. https://doi.org/10.1039/c2jm32343e.

[28] N. Bhuvanesh, S. Suresh, K. Kannan, V. Rajesh Kannan, N. Maroli, P. Kolandaivel, R. Nandhakumar, Bis-anthracene derived bis-pyridine: selective fluorescence sensing of Al 3+ ions †, New J. Chem. 43 (2019) 2519. https://doi.org/10.1039/c8nj04789h.

[29] D. Bawari, C. Negi, V. Kumar Porwal, S. Ravi, K.R. Shamasundar, S. Singh, Aluminum containing molecular bowls and pyridinophanes: use of pyridine modules to access different molecular topologies, Dalt. Trans. 48 (2019) 7442. https://doi.org/10.1039/c8dt05105d.

[30] J. Molina-Reyes, H. Uribe-Vargas, R. Torres-Torres, P.G. Mani-Gonzalez, A. Herrera-Gomez, Accurate modeling of gate tunneling currents in Metal-Insulator-Semiconductor capacitors based on ultra-thin atomic-layer deposited Al2O3 and post-metallization annealing, Thin Solid Films. 638 (2017) 48–56. https://doi.org/10.1016/j.tsf.2017.07.031.

[31] E.P. Gusev, E. Cartier, D.A. Buchanan, M. Gribelyuk, M. Copel, H. Okorn-Schmidt, C. D'Emic, Ultrathin high-K metal oxides on silicon: Processing, characterization and integration issues, in: Microelectron. Eng., 2001: pp. 341–349. https://doi.org/10.1016/S0167-9317(01)00667-0.

[32] A. Herrera-Gomez, M. Bravo-Sanchez, O. Ceballos-Sanchez, M.O. Vazquez-Lepe, Practical methods for background subtraction in photoemission spectra, Surf. Interface Anal. 46 (2014) 897–905. https://doi.org/10.1002/sia.5453.

[33] A. HERRERA-GOMEZ, Y. SUN, F.-S. AGUIRRE-TOSTADO, C. HWANG, P.-G. MANI-GONZALEZ, E. FLINT, F. ESPINOSA-MAGAÑA, R.M. WALLACE, Structure of Ultra-Thin Diamond-Like Carbon Films Grown with Filtered Cathodic Arc on Si(001), Anal. Sci. 26 (2010) 267–272. https://doi.org/10.2116/analsci.26.267.

[34] J.R. Shallenberger, Determination of chemistry and microstructure in SiO x (0.1< x <0.8) films by x-ray photoelectron spectroscopy , J. Vac. Sci. Technol. A Vacuum, Surfaces, Film. 14 (2002) 693–698. https://doi.org/10.1116/1.580373.

[35] M.T. Rodgers, J.R. Stanley, R. Amunugama, Periodic Trends in the Binding of Metal Ions to Pyridine Studied by Threshold Collision-Induced Dissociation and Density Functional Theory, (2000). https://doi.org/10.1021/ja0027923.

[36] P. Satyanarayan, Pyridine: A Useful Ligand in Transition Metal Complexes, in: Intech, London, 2016: pp. 57–74. https://doi.org/http://dx.doi.org/10.5772/57353.

[37] A. Kundu, J. Pitchaimani, V. Madhu, P. Sakthivel, R. Ganesamoorthy, & Savarimuthu, P. Anthony, Bay Functionalized Perylenediimide with Pyridine Positional Isomers: NIR Absorption and Selective Colorimetric/Fluorescent Sensing of Fe 3+ and Al 3+ Ions, (1976). https://doi.org/10.1007/s10895-016-1976-z.

[38] P.G. Mani-Gonzalez, M. Snelgrove, J. Rueff, R. Lundy, P. Yadav, J. Bogan, R. O'Connor, M. Morris, G. Hughes, Analysis of Al and Cu salt infiltration into a poly 2- vinylpyridine (P2vP) polymer layer for semiconductor device patterning applications, (n.d.) 1–20.

[39] F.J. Himpsel, F.R. McFeely, A. Taleb-Ibrahimi, J.A. Yarmoff, G. Hollinger, Microscopic structure of the SiO2/Si interface, Phys. Rev. B. 38 (1988) 6084–6096. https://doi.org/10.1103/PhysRevB.38.6084.

[40] I. Menapace, W. Yiming, E. Masad, Chemical analysis of surface and bulk of asphalt binders aged with accelerated weathering tester and standard aging methods, Fuel. 202 (2017) 366–379. https://doi.org/10.1016/j.fuel.2017.04.042.

[41] K. Wright, A. Barron, Catalyst Residue and Oxygen Species Inhibition of the Formation of Hexahapto-Metal Complexes of Group 6 Metals on Single-Walled Carbon Nanotubes, C. 3 (2017) 17. https://doi.org/10.3390/c3020017.

[42] F.S. Aguirre-Tostado, M. Milojevic, B. Lee, J. Kim, R.M. Wallace, In situ study of surface reactions of atomic layer deposited Lax Al2-x O3 films on atomically clean In0.2 Ga0.8 As, Appl. Phys. Lett. 93 (2008) 1–4. https://doi.org/10.1063/1.3009303.

[43] J.X. Liao, L.F. Xia, M.R. Sun, W.M. Liu, T. Xu, C.R. Yang, H.W. Chen, C.L. Fu, W.J. Leng, Structural characteristics of 2024 aluminum alloy plasma-based ion implanted with nitrogen then titanium, (2004). https://doi.org/10.1016/j.apsusc.2004.06.145.

[44] B.V. Crist, Handbooks of Monochromatic XPS Spectra Volume 2-Commercially Pure Binary Oxides (Ag-B, Zn-Zr only) and a few Common Carbonates and Hydroxides Handbooks of Monochromatic XPS Spectra Volume Two-Commercially Pure Binary Oxides 1, XPS International LLC, Mountain View, 2005. www.xpsdata.com.

[45] T. Gougousi, † Dipak Barua, E.D. Young, G.N. Parsons, Metal Oxide Thin Films Deposited from Metal Organic Precursors in Supercritical CO 2 Solutions, (2005). https://doi.org/10.1021/cm0510965.

[46] J. Andrés, P. Taborda, L.P. Vera, Correlation between optical , morphological and compositional properties of Aluminum Nitride thin films by Pulsed Laser Deposition, IEEE Sens. J. (2015). https://doi.org/10.1109/JSEN.2015.2466467.

[47] I. Iatsunskyi, M. Kempiński, M. Jancelewicz, K. Załęski, S. Jurga, V. Smyntyna, Structural and XPS characterization of ALD Al2O3 coated porous silicon, Vacuum. (2015). https://doi.org/10.1016/j.vacuum.2014.12.015.

[48] G. Faraci, S. La Rosa, A.R. Pennisi, Y. Hwu, G. Margaritondo, Al intermediate oxidation states observed by core level photoemission spectroscopy, J. Appl. Phys. 78 (1995) 4091–4098. https://doi.org/10.1063/1.359866.